Available online at www.sciencedirect.com

SciVerse ScienceDirect

Advances in Space Research 51 (2013) 849–857

ADVANCES IN SPACE RESEARCH (a COSPAR publication)

www.elsevier.com/locate/asr

Autonomous navigation of Mars probe using X-ray pulsars: Modeling and results

Erhu Wei [a,1], Shuanggen Jin [b,*], Qi Zhang [c,a], Jingnan Liu [d], Xuechuan Li [a], Wei Yan [a]

[a] School of Geodesy and Geomatics, Wuhan University, Wuhan 430079, China
[b] Shanghai Astronomical Observatory, Chinese Academy of Sciences, Shanghai 200030, China
[c] Tianjin Institute of Surveying and Mapping, Tianjin 300381, China
[d] GNSS Research Center, Wuhan University, Wuhan 430079, China

Received 6 August 2012; accepted 10 October 2012
Available online 22 October 2012

Abstract

Autonomous navigation of Mars probe is a main challenge due to the lack of dense ground tracking network measurements. In this paper, autonomous navigation of the Mars probe Orbits is investigated using the X-ray pulsars. A group of X-ray pulsars with high ranging accuracy are selected based on their properties and an adaptive extended Kalman filter is developed to incorporate the Mars probe dynamics and pulsar-based ranging measurements. Results of numerical experiment show that the three-dimensional positioning accuracy can achieve 750m in X-axis, 220m in Y-axis and 230m in Z-axis, which is much better than the positioning results by current Very Long Baseline Interferometry (VLBI) or Doppler observations with the accuracy of 150 km or several kilometers, respectively.

Keywords: Autonomous navigation; Mars exploration; Adaptive Kalman filter; X-Ray navigation

1. Introduction

Mars exploration is an important step for deep space exploration, including space environments, origin, formation and evolution, internal structure and possible life of planets. Navigation and positioning of Mars probes are essential for implementing Mars exploration successfully. The probe failure of "Phobos-Grunt" just launched by Russia demonstrates the importance of the autonomous navigation of Mars probe. Traditional methods used for the deep space exploration need ground based stations for tracking, observation and communication, such as VLBI and Doppler tracking for lunar probe, while the positioning accuracy is about 150 km and several km respectively (Li et al., 2010; Cao et al., 2010) . On the other hand, the distance between Mars probe and Earth is a great challenge for VLBI and Doppler tracking. So, autonomous navigation of Mars probe is currently urgent and also compensates the defects of the traditional techniques, e.g., reducing the dependence on ground tracking stations and increasing the successful navigation for Mars exploration.

X-ray pulsar navigation and positioning technology has a huge potential as the dawn of the deep space probe's autonomous navigation. In this paper, the autonomous navigation of Mars probe based on X-ray pulsars is investigated. The related coordinate systems and their interconnections will be introduced in Section 2. A group of X-ray pulsars with high ranging accuracy will be selected based on their properties and an adaptive extended Kalman filter will be developed to incorporate the Mars probe dynamics and pulsar-based ranging measurements in Section 3. Numerical experiment and test results will be presented in Section 4 and finally conclusions are given in Section 5.

* Corresponding author. Tel.: +86 21 34775292.
E-mail addresses: sgjin@shao.ac.cn (S. Jin), jnliu@whu.edu.cn (J. Liu), leexc0124@163.com (X. Li).
[1] Tel.: +86 27 68758505

0273-1177/$36.00
http://dx.doi.org/10.1016/j.asr.2012.10.009

2. Related coordinate systems

Coordinate systems involved in autonomous navigation based on X-ray pulsars include the Barycentric Coordinate System (S_{SB}), Mars-centered Mean Equator and Equinox Coordinate System (S_{MCI}), and Mars-Centered Inertial Coordinate System (S_{ECI}). The specific definition of the coordinate systems mentioned above can be referred to (Wei and Xu, 2009; Brukhart 2006). The interconnections of these coordinate systems are given by Eqs. (1)–(3).

$$R_{SB} = R_{ECI} + R_M \tag{1}$$

$$R_{ECI} = R_{MCI2ECI} R_{MCI} \tag{2}$$

$$R_{MCI2ECI} = R_2(F) \cdot R_x(I) \cdot R_z(E) \tag{3}$$

where $R_{MCI2ECI}$ is the interconnection matrix from S_{MCI} to S_{ECI}. R_{SB} is the position vector of the probe in S_{SB}. R_{ECI} is the position of the probe in S_{ECI}. R_{MCI} is the position of the probe in S_{MCI}. R_M is the position of the center of Mars in S_{SB}, which can be obtained from JPL's DE414. F, I and E are the Euler angles from R_{MCI} to S_{ECI}, which can also be obtained from DE414.

As the dynamic model of Mars probe is described in R_{MCI} but the observation of pulsars is described in S_{ECI}, the time prediction model of the pulsar must be transformed from the barycenter of solar system to the center of Mars and the accuracy of the transformation is 0.1 μs (Sheikh, 2005). Figure. 1 shows the geometry of spacecraft navigation using X-ray Pulsars (Chiaradia et al., 2008), where SSB is the solar system barycenter, RM is the vector from SSB to the centre of Mars, RMCI is the vector from the center of Mars to the Mars probe, and RSB is the vector from SSB to the center of Mars.

3. Adaptive extended Kalman filter

The blending of probe state dynamics and pulse ranging measurement can be implemented using an extended Kalman filter technique. This filter, referred to as the Navigation Kalman Filter, recursively incorporates pulse ranging measurements with an estimate of the orbit state. The estimated states are based upon a numerically propagated position and velocity solution. In order to achieve better accuracy of the solution and faster convergence, method of adaptive extended Kalman filtering is used for the autonomous navigation.

3.1. The dynamic model

The problem of dynamical orbit determination of Mars probe in the Mars orbit is essentially nonlinear. The orbital components are described in the inertial frame S_{MCI} by a set of ordinary differential equations.

$$\ddot{r} = -\frac{\mu M^r}{r^3} + a + W \tag{4}$$

where r is the position component vector of the probe (x, y, z), μ_M is the gravity parameter of Mars, W is the white noise vector with a covariance of Q, and a is the modeled perturbing accelerations. Because the Martian J_2 is the major perturbing factor (Liu and Tang, 2008), in this dynamic model, only J_2 perturbing accelerations are taken into account as.

$$a_r = aJ_2 \tag{5}$$

Where

$$aJ_2 = \begin{bmatrix} -\frac{\mu M^x}{r^3} J_2 \left(\frac{R_m}{r}\right)^2 \frac{3}{2}\left(1 - 5\frac{z^2}{r^2}\right) \\ -\frac{\mu My}{r^3} J_2 \left(\frac{R_m}{r}\right)^2 \frac{3}{2}\left(1 - 5\frac{z^2}{r^2}\right) \\ -\frac{\mu M^z}{r^3} J_2 \left(\frac{R_m}{r}\right)^2 \frac{3}{2}\left(3 - 5\frac{z^2}{r^2}\right) \end{bmatrix} \tag{6}$$

Thus, the state vector to be estimated is defined as following

$$X = [r, \upsilon]^T \tag{7}$$

where υ is the velocity vector of Mars probe. Thus, the dynamic model can be expressed:

$$\dot{X} = f(X, t) + W \tag{8}$$

Under an initial state of the probe, the next state can be numerically integrated with Eq. (8). The system described by Eq. (8) is non-linear which makes it impossible to apply one of the well-known methods of sequential linear estimation, the Kalman Filter. The extended Kalman filter is a Kalman filter version applicable for non-linear problems such as this one, composed by a time-updated and a measurement updated cycles. After linearization the sensitive equation can be written as (Shuai et al., 2010):

$$\delta\dot{X}(t) = F(t)\delta X(t) + W(t) \tag{9}$$

where $F(t) = \frac{\partial f[X(t),t]}{\partial X(t)}\big|_{X(t)=\hat{X}^n(t)}$, $F(t)$ is the Jacobian Matrix of the system, and $\hat{X}^n(t)$ is the one step optimal estimation of

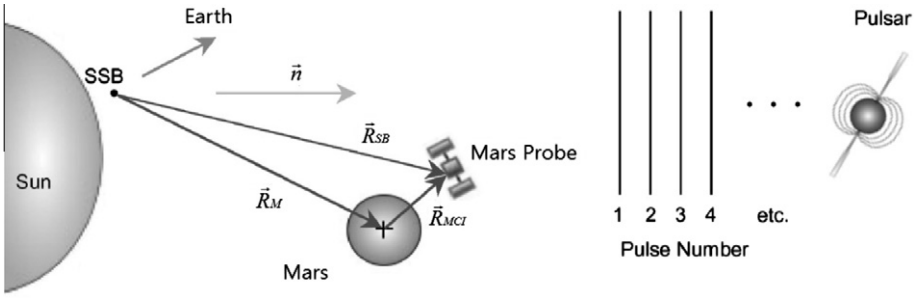

Fig. 1. Geometry of Mars probe navigation using X-ray pulsars (Graven et al., 2008).

state calculated by numerical propagation at t. By discretization, Eq. (9) can be rewritten as:

$$\delta X_k = \Phi_{k,k-1}\delta X_{k-1} + W_{k-1} \tag{10}$$

where $\Phi_{k,k-1}$ is the Transition matrix which relates the state between t_k and t_{k-1}.

3.2. Calculation of transition matrix

Due to the limitation of the computing speed and memory of on-board computer, here the Markley's method is applied for calculating the Transition matrix. Components for the calculation of Transition matrix used in Markley's method are the status of the probe in time t_k and time t_{k-1}, μM, J_2, Δt, the radius of the Mars, and so on. The effect of the Mars' oblateness is the most influent factor in the process. Markley's method consists of one approximation for the Transition matrix of the state vector based on the Taylor series expansion at short intervals of propagation, Δt. According to Markley's Method, the Transition matrix of the state with some simplifications is given as

$$\Phi(t,t_0) \approx \begin{bmatrix} \Phi_{rr} & \Phi_{rv} \\ \Phi_{vr} & \Phi_{vv} \end{bmatrix}_{6\times 6} \tag{11}$$

where $\Phi(t_0,t_0) = I$ is the initial condition, and

$$\begin{aligned} \Phi_{rr} &= I + (2G_0 + G)\frac{(\Delta t)^2}{6} \\ \Phi_{rv} &= I\Delta t + (G_0 + G)\frac{(\Delta t)^3}{12} \\ \Phi_{vr} &= (G_0 + G)\frac{(\Delta t)}{2} \\ \Phi_{vv} &= I + (G_0 + 2G)\frac{(\Delta t)^2}{6} \\ \Delta t &= t - t_0 \end{aligned} \tag{12}$$

There are no problems in the calculation of these matrices because the gradient matrix G in the end of the propagating interval is a function of the final state, which is known after numerical propagation (Markley, 1986; Chiaradia and Kuga, 2012). If only J_2 of the center body is considered (Moraes, 2007), the matrix G can be given by

$$G(t) = \frac{\partial a(r,t)}{\partial r} = \begin{bmatrix} \frac{\partial a_x}{\partial x} & \frac{\partial a_x}{\partial y} & \frac{\partial a_x}{\partial z} \\ \frac{\partial a_y}{\partial x} & \frac{\partial a_y}{\partial y} & \frac{\partial a_y}{\partial z} \\ \frac{\partial a_z}{\partial x} & \frac{\partial a_z}{\partial y} & \frac{\partial a_z}{\partial z} \end{bmatrix} \tag{13}$$

$$\begin{aligned} a_x &= -\frac{\mu M^x}{r^3}\left[1 + \frac{3}{2}\frac{J_2R_m^2}{r^2}(1 - \frac{5z^2}{r^2})\right] \\ a_y &= \frac{y}{x}a_x \\ a_z &= -\frac{\mu Mz}{r^3}\left[1 + \frac{3}{2}\frac{J_2R_m^2}{r^2}\left(3 - \frac{5z^2}{r^2}\right)\right] \end{aligned} \tag{14}$$

In Eq. (13), $a(r,t)$ is the acceleration of the probe. The partial derivatives are

$$\begin{aligned} \frac{\partial a_x}{\partial x} &= \frac{\mu M}{r^3}\left[3x^2 - r^2 - \frac{3}{2}J_2R_m^2 + \frac{15}{2}\frac{J_2R_m^2}{r^2}(x^2+z^2) - \frac{105}{2}\frac{J_2R_m^2}{r^4}x^2z^2\right] \\ \frac{\partial a_x}{\partial y} &= \frac{3\mu Mxy}{r^5}\left[1 + \frac{5}{2}\frac{J_2R_m^2}{r^2} - \frac{35}{2}\frac{J_2R_m^2}{r^4}z^2\right] \\ \frac{\partial a_x}{\partial z} &= \frac{3\mu Mxz}{r^5}\left[1 + \frac{15}{2}\frac{J_2R_m^2}{r^2} - \frac{35}{2}\frac{J_2R_m^2}{r^4}z^2\right] \\ \frac{\partial a_y}{\partial x} &= \frac{\partial a_x}{\partial y} \\ \frac{\partial a_y}{\partial y} &= \frac{y}{x}\frac{\partial a_x}{\partial z} + \frac{a_x}{x} \\ \frac{\partial a_y}{\partial z} &= \frac{y}{x}\frac{\partial a_x}{\partial z} \\ \frac{\partial a_z}{\partial x} &= \frac{\partial a_x}{\partial z} \\ \frac{\partial a_z}{\partial y} &= \frac{\partial a_y}{\partial z} \\ \frac{\partial a_z}{\partial z} &= \frac{\mu M}{r^5}\left[-r^2 + 3\left(z^2 - \frac{3}{2}J_2R_m^2 + 15\frac{J_2R_m^2}{r^2}z^2 - \frac{35}{2}\frac{J_2R_m^2}{r^4}z^4\right)\right] \end{aligned} \tag{15}$$

where R_m is the radius of the Mars; $r = (x,y,z)^T$, $v = (\dot{x},\dot{y},\dot{z})^T$ are the position and velocity of the probe in R_{MC}, and μM is the gravity parameter of Mars.

3.3. The measurement model

The measurement model of the Kalman filter algorithm is expressed as:

$$Z_k = H_kX_k + V_k \tag{16}$$

where Z is the observation of pulsars and V is the white noise vector that represents the random errors of the measurements modeled by

$$E[V_k] = 0 \tag{17}$$

$$E(V_kV_j^T) = R_k\delta_{kj} \tag{18}$$

where δ_{kj} is the Kronecker delta equals to 1 when $k = j$ and zero otherwise, V can be given by the accuracy of the ranging measurement based on X-ray pulsars and R is the covariance of V. H_k is the function of state X_k, according to the theory of X-ray pulsars navigation, which can be expressed by

$$H_k = \begin{bmatrix} n_1^TR_{MCI2ECI}R_{MCI1} & 0_{1\times 3} \\ n_2^TR_{MCI2ECI}R_{MCI2} & 0_{1\times 3} \\ n_3^TR_{MCI2ECI}R_{MCI3} & 0_{1\times 3} \\ \cdots & \cdots \\ n_j^TR_{MCIjECI}R_{MCIj} & 0_{1\times 3} \end{bmatrix} \tag{19}$$

where n^T is the direction vector of the pulsar in S_{ECI}. For the long distance from the pulsar to the Mars, n^T in S_{ECI} can be considered the same as in S_{SB}, and $R_{MCI2ECI}$ is as Eq. (3).

3.4. The adaptive extended Kalman filter

In order to achieve better accuracy of the solution and faster convergence, method of adaptive extended Kalman filtering is used in this paper. The process of the adaptive extended Kalman filter is showing below.

The one step optimal predicting state is calculated by

$$\widehat{X}_{k/k-1} = \widehat{X}_{k-1} + f(\widehat{X}_{k-1}, t_{k-1})\Delta t \tag{20}$$

The covariance of the one step optimal predicting state is calculated by

$$P_{k/k-1} = \Phi_{k/k-1} P_{k-1} \Phi_{k,k-1}^T + Q_{k-1} \tag{21}$$

where Q is the covariance of W. The adaptive factor is calculated by

$$\sigma_k = \left[\frac{tr(\hat{Q}_R)}{tr(Q_R)}\right]^{\frac{1}{2}} \tag{22}$$

where $\hat{Q}_R$ and Q_R are the covariance of the predicted residuals and the theoretical residuals of the observations, respectively. The optimal Kalman gain matrix is calculated by

$$K_k = \frac{1}{\alpha_k} P_{k/k-1} H_k^T \left(\frac{1}{\sigma_k} H_k P_{k/k-1} H_k^T + R_k\right)^{-1} \tag{23}$$

The optimal filtering state is calculated by

$$\hat{X}_k = \widehat{X}_{k/k-1} + K_k[Z_k - h(\widehat{X}_{k/k-1}, k)] \tag{24}$$

The covariance of the optimal filtering state is calculated by

$$P_k = (I - K_k H_k) P_{k/k-1} (I - K_k H_k)^T + K_k R_k K_k^T \tag{25}$$

4. Numerical experiment

To verify the performance of the autonomous navigation based on X-ray pulsars, numerical experiment is carried out based on the adaptive extended Kalman filter mentioned above.

4.1. Analysis of ranging accuracy

In order to select the pulsars for the autonomous navigation of the Mars probe, the ranging accuracy of pulsars has been analyzed based on their properties. Ranging accuracy of the pulsar can be expressed as (Chiaradia et al., 2012):

$$\sigma_r = c\sigma_{TOA} \tag{26}$$

$$\sigma_{TOA}^2 = \frac{W_{50\%}^2}{(SNR)^2} = \frac{[B_x + F_X(1-pf)]ATd + F_X A_p f T}{(F_X A_{pf} T)^2} W_{50\%}^2 \tag{27}$$

where σ_r is the ranging accuracy of the pulsar, σ_{TOA} is the TOA measuring accuracy of the pulsar, SNR is the Signal to Noise Ratio of the pulse signal, B_X is the X-ray background radiation flux, F_X is the observed X-ray photon flux, A is the area of the detector, T is the observation time, pf is the pulsar's parameter of pulsed fraction, d is the duty cycle of the pulsar, $W_{\%50}$ is the half width of the pulse, and c is the speed of the light. Here, 25 ms pulsars are selected for the analysis of the ranging accuracy, which are from ATNF pulsar database, Chandra ACIS Detector pulsar database and XNAVSC (Sheikh, 2005). The parameters of pulsars in experiment are from pulsar databases (Ray et al., 2008; Kargaltsev et al., 2012; Barry et al., 2012). In the analysis, A is set to 4m^2, and B_X is set to $0.005\text{ph/cm}^2\text{/s}$ which is a common value. With analysis, seven pulsars with better ranging accuracy are selected as the navigation stars in the numerical experiment. The ranging accuracy of the seven pulsars is shown as Fig. 2.

Table 1 lists the ranging accuracy of the seven pulsars. Analysis shows the ranging accuracy is becoming better when the observation time is longer. Taking into account that long time predicting without correction of the observations may cause too large deviation of the state solution of the probe, in the numerical experiment, the observation time will be set to 500 s.

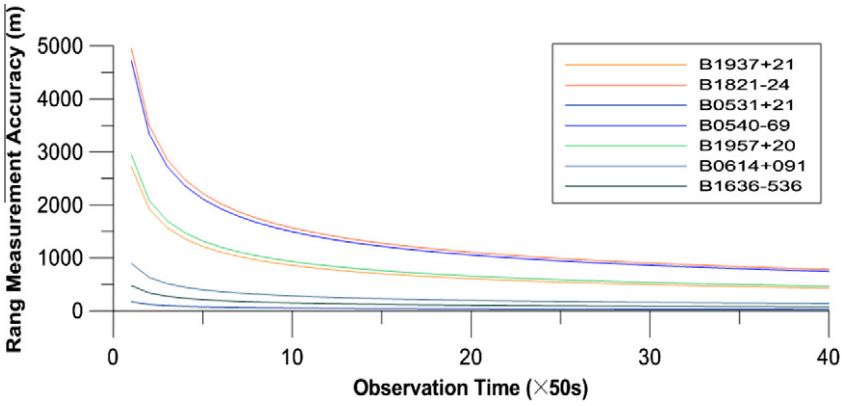

Fig. 2. Relationship between observation time and ranging accuracy.

Table 1
Ranging accuracy with observation time.

Obs time (s)	B1937 +21 (m)	B1821 –24 (m)	B0531 +21 (m)	B0540 –69 (m)	B1957 +20 (m)	B0614 +091 (m)	B1636 –536 (m)
500	860	156	54	1493	932	282	151
1000	608	1107	38	1056	659	199	106
1500	496	904	31	862	538	163	87
2000	430	783	27	746	466	141	75

Table 2
Mars parameters for observations simulation.

Central body	Gravity model	Planet eph	Gm ($10^6 km^3/s^2$)	J_2 (10^{-6})	Radius (km)
Mars	GMM2B	DE414	0.3986	1960.45	3397

Table 3
Initial orbital elements of the Mars probe.

e	a	i	Ω	w	M_0
15000 km	0.005	30°	30°	30°	0°

4.2. Observations simulation

The parameters of Mars (Lemoine et al., 2001) used for observations simulation is listed in Table 2.

The probe's orbit for X-ray pulsar observation is simulated with the Satellite Tool Kit (STK). And the orbit simulated with STK is also considered as the nominal orbit for the outer accuracy assessment. The initial orbit elements of the Mars probe for observations simulation is listed in Table 3.

In the observation simulation, the error of on-board clock and the error of transformation of the pulsar time model from the barycenter of Solar System to the center of Mars are taken into consideration. The clock bias and transformation error are set to 10^{-9} s and 10^{-7} s, respectively (Sheikh, 2005).

4.3. Filtering

Based on the adaptive Kalman filter model derived above and the simulated pulsar observations, numerical

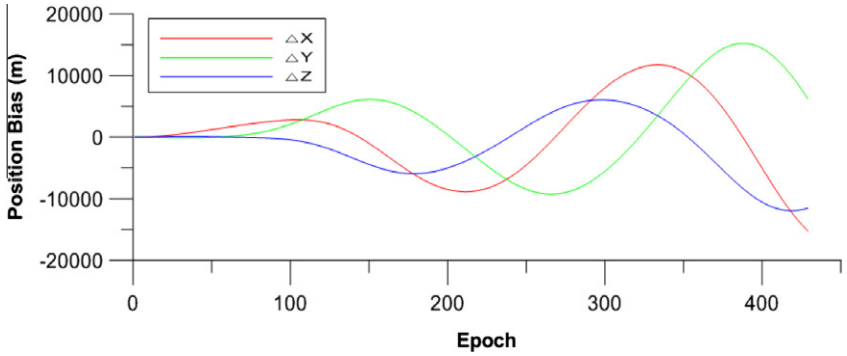

Fig. 3. Position bias between RKF7(8) orbit and nominal orbit.

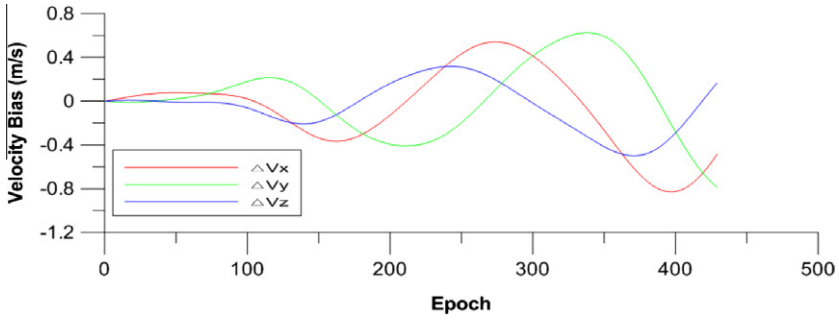

Fig. 4. Velocity bias between RKF7(8) orbit and nominal orbit.

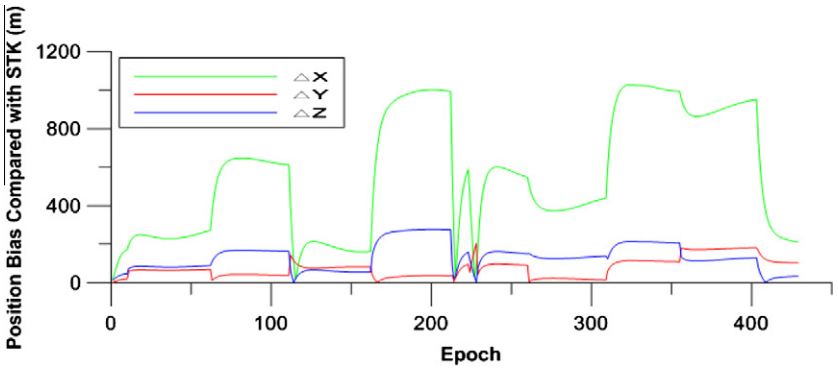

Fig. 5. Position bias between filtering orbit and nominal orbit.

experiment is taken to verify the performance of the autonomous navigation based on X-ray pulsars. The initial parameters of the filtering are set with $R_0 = diag[(860\text{m})^2(1560\text{m})^2(54\text{m})^2(1493\text{m})^2(932\text{m})^2 (282\text{m})^2(151\text{m})^2]$, $Q_0 = diag[(0.54\text{m})^2(0.5\text{m})^2(0.5\text{m})^2 (0.005\text{m/s})^2(0.0001\text{m/s})^2(0.0001\text{m/s})^2]$ and $P_{0/0} = diag[(100\text{m})^2(100\text{m})^2(100\text{m})^2(0.1\text{m/s})^2(0.08\text{m/s})^2 (0.05\text{m/s})^2]$

The numerical propagator for the one-step status prediction in this paper is RKF7(8). Fig. 3 is the 3-dimensional position bias between the orbit predicted by RKF7(8) and STK nominal orbit and Fig. 4 is the 3-dimensional velocity bias between the RKF7(8) orbit and the STK orbit, which both show that the orbit bias increases heavily with epoch increasing.

Fig. 5 shows the 3-dimensional position solution after adaptive Kalman filtering indicating that with the epoch increasing, the bias between filtering position and nominal position is less than 1 km in X-axis, 200 m in Y-axis and Z-axis. Fig. 6 is the accuracy of the 3-dimensional position solution after adaptive Kalman filtering. It illustrates that with the epoch increasing, the accuracy of the position is less than 750 m in X-axis, 220 m in Y-axis and 230 m in Z-axis.

Fig. 7 describes the 3-dimensional velocity solution after adaptive Kalman filtering and illustrates that with the epoch increasing, the bias between filtering velocity and nominal velocity is within 0.16 m/s in X-axis, 0.10 m/s in Y-axis and 0.08 m/s in Z-axis.

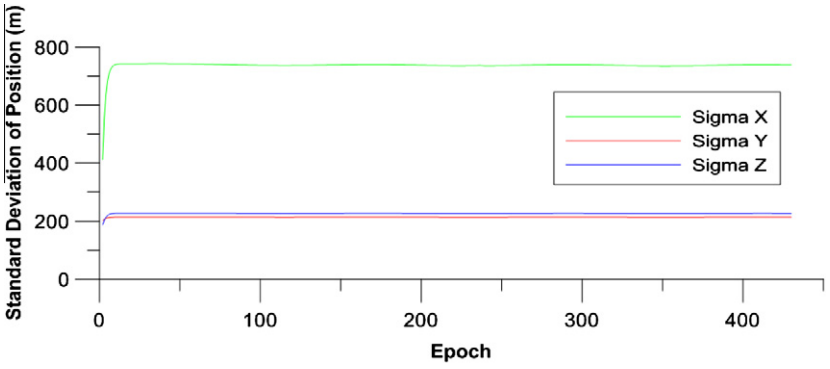

Fig. 6. Position accuracy of the filtering orbit.

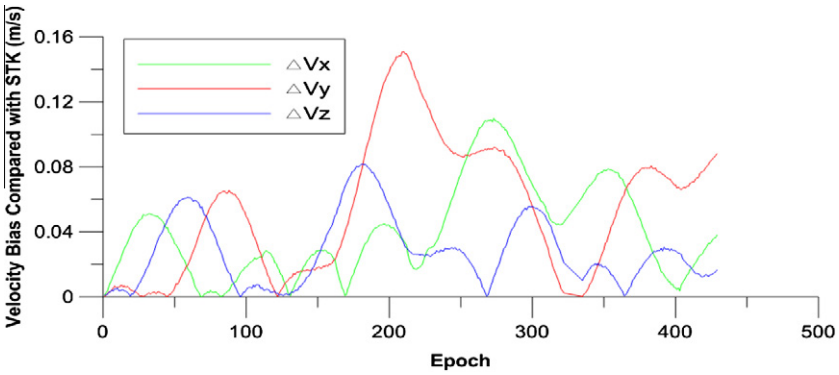

Fig. 7. Velocity bias between filtering orbit and nominal orbit.

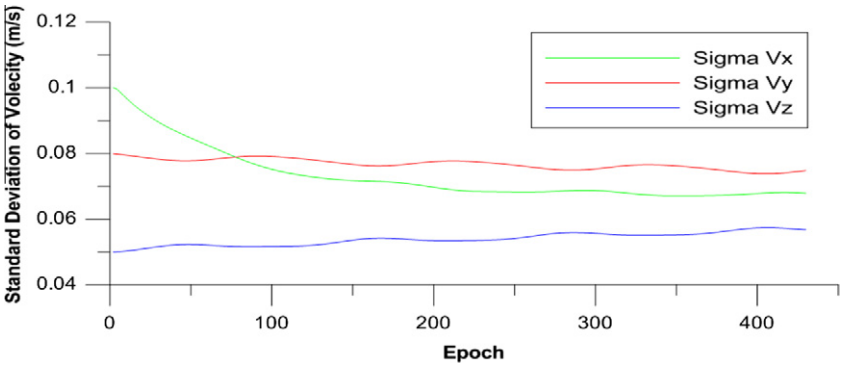

Fig. 8. Velocity accuracy of the filtering orbit.

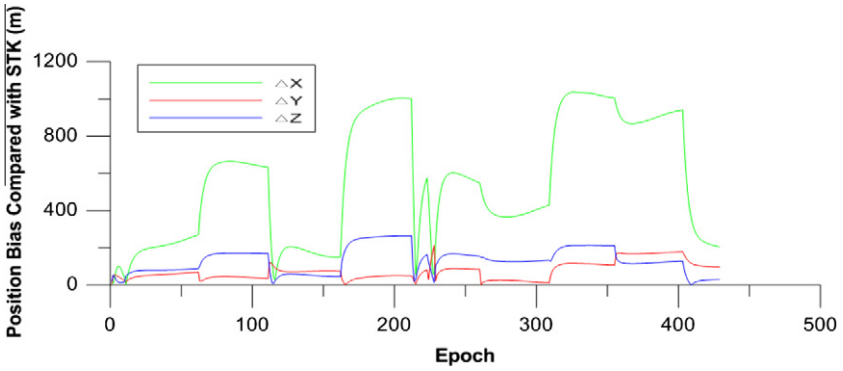

Fig. 9. Position bias between filtering orbit with initial error and nominal orbit.

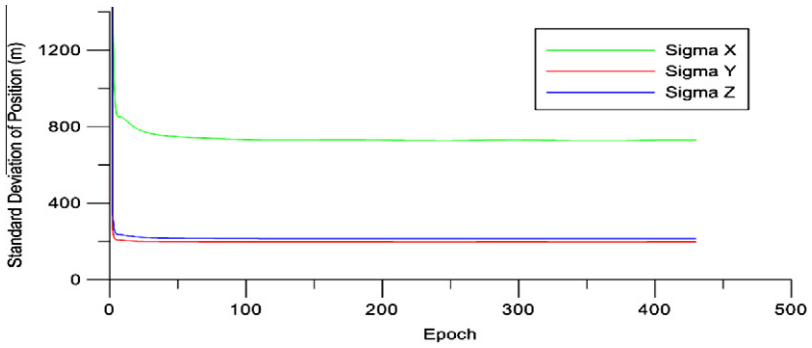

Fig. 10. Position accuracy of the filtering orbit with initial error.

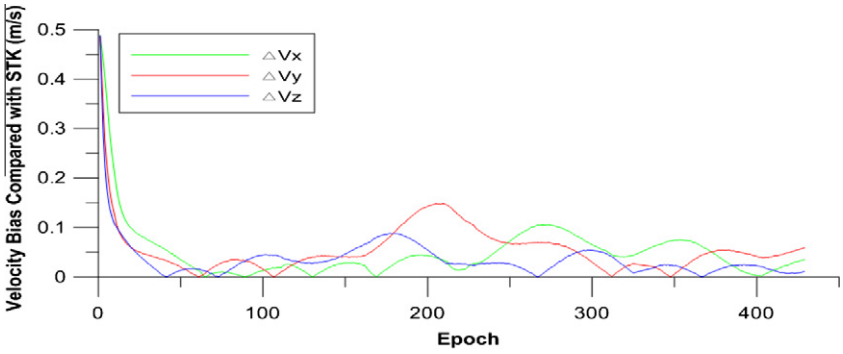

Fig. 11. Velocity bias between filtering orbit with initial error and nominal orbit.

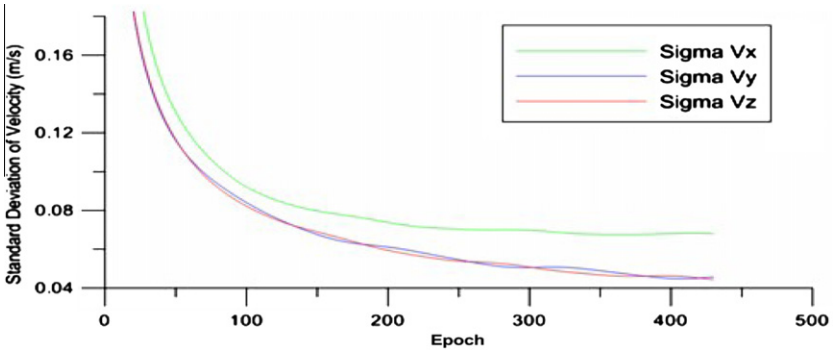

Fig. 12. Velocity accuracy of the filtering orbit with initial error.

Fig. 8 is the accuracy of velocity solution after adaptive Kalman filtering, showing that with the epoch increasing, the accuracy of the velocity is within 0.07 m/s in X-axis, 0.075 m/s in Y-axis and 0.06 m/s in Z-axis.

In most situations, the initial state of the probe cannot be completely accurate. For investigating the influence of the initial state error on the autonomous navigation based on X-ray pulsars, 10 km initial position error on each axis and 0.5 m/s initial velocity error on each axis are set as the initial state of the probe. Fig. 9 is the position bias between filtering orbit with initial error and nominal orbit and Fig. 10 is the accuracy of the position solution after adding 10 km initial position error. It demonstrates that after about 5 or 6 epochs, the accuracy of the position solution converges rapidly to 750 m in X-axis, 220 m in Y-axis and 230 m in Z-axis.

Fig. 11 is the velocity bias between filtering orbit with initial error and nominal orbit and shows that as epoch increasing, the velocity bias is decreasing at the first 50 epochs, but then, becomes steadily within 0.1 m/s.

Fig. 12 is the accuracy of the velocity solution with initial error, which demonstrates that with epoch increasing, the accuracy of the velocity solution is getting better and better. Finally, the accuracy is achieved 0.07 m/s in X-axis, 0.043 m/s in Y-axis and Z-axis. It also shows that it takes longer time for convergence than the accuracy of position solution.

5. Conclusions

Theoretical analysis and numerical simulation above show that autonomous navigation of the Mars probe in the Mars orbit based on X-ray pulsar performs well. The results demonstrate that the accuracy of the position after filtering can achieve 750 m in X-axis, 220 m in Y-axis and 230 m in Z-axis, which is much better than VLBI or Doppler positioning solution with the accuracy of about 150 km or several km, respectively. The perturbations of the Mars' atmospheric, solar radiation pressure and higher order gravity field of Mars are not taken into account in the dynamical model of the Mars probe in the Mars orbit. In the future, to increase the accuracy of the autonomous navigation of the Mars probe based on X-ray pulsar, we will further carefully consider those perturbations effects.

Acknowledgments

This research is funded by the National 863 Project of China (Grant No.2008AA12Z308), the National Natural Science Foundation of China (Grant No. 40974003), National Basic Research Program of China (973 Program) (Grant No. 2012CB720000) and Main Direction Project of Chinese Academy of Sciences (Grant No. KJCX2-EW-T03).

References

Li, J.L., Liu, P., Ma, M., et al. Positioning reduction of the mars express tracking data by the Chinese VLBI network. J. Astronaut. 31 (7), 1718–1723, 2010.

Cao, J.F., Huang, Y., Hu, X., et al. Mars Express tracking and orbit determination trails with Chinese VLBI network. Chin. Sci. Bull. 55, 3654–3660, 2010.

Wei, J., Xu, S. Analysis on the influence of natural convection during melting of phase change material. Chinese Space Sci. Tech. 29 (2), 65–70, 2009.

Brukhart. P.D. MSL Update to Mars Coordinate Frame Definitions [EB/OL]. <http://www.coursehero.com/file/2541877/HW4/.2006-08-15:1-20>, 2006.

Sheikh, S.I., The use of variable celestial X-ray sources for spacecraft for navigation[D], Department of Aerospace Enginerring University of Maryland, Maryland, 2005.

Liu, L., Tang, J. Orbit variation characteristics of the mars' orbiters. J. Astronaut. 29 (2), 461–466, 2008.

Shuai, P., Li, M., Chen, S., Huang, Z. The theory and method of the X-ray pulsar navigation system[M]. Chinese Astronautics Press, Beijing, 2010.

Moraes, R.V.A.A., Silva, H., Kuga, K Simple orbit determination using GPS based on a least-squares algorithm employing sequential given rotations. Math. Prob. Eng. 10 (49781), 1–8, 2007.

Markley, J. Approximate cartesian state transition matrix. J. Astronaut. Sci. 34 (2), 161–169, 1986.

Chiaradia, A.P.M., Kuga, H.K. Comparision between two methods to calculate the transition matrix of orbit motion. mathematical problems in engineering. Math. Prob. Eng. 10, 768973, 2012.

Ray, P.S., Sheikh, S.I., Graven, P.H., Wolff, M.T., Wood, K.S., Gendreau, K.C. Deep space navigation using celestial X-ray sources. ION NTM 28 (30), 101–109, 2008.

Kargaltsev, O. et al. X-ray Pulsars Database [EB/OL]. <http://www2.astro.psu.edu/users/green/psrdatabase>, 2012.

Barry.T. et al. ATNF Pulsar Catalogue [EB/OL]. <http://www.atnf.csiro.au/research/pulsar/psrcat/>, 2012.

Lemoine, F.G., Smith, D.E., Rowlands, D.D., Zuber, M.T., Neumann, G.A., Chinn, D.S. An improved solution of the gravity field of Mars from Mars global surveyer. J Geophys. Res. 106 (E10), 23359–23376, 2001.

Graven, P. H., Collins, J.T., Sheikh, S.I., Hanson, J.E., Spacecraft navigation using X-ray pulsars. In: Seventh International ESA Conference on Guidance, Navigation & Control Systems. pp. 1–17, 2008.